Prepared for submission to JHEP IFIC/15-43

Single bottom quark production in $k_\perp$-factorisation

Grigorios Chachamis[a], **Michal Deák**[b], **Martin Hentschinski**[c], **Germán Rodrigo**[b] **and Agustín Sabio Vera**[a]

[a] *Instituto de Física Teórica UAM/CSIC & Universidad Autónoma de Madrid, C/ Nicolás Cabrera 15, E-28049 Madrid, Spain*

[b] *Institut de Física Corpuscular, Universitat de València – Consejo Superior de Investigaciones Científicas, Parc Científic, 46980 Paterna, València, Spain*

[c] *Instituto de Ciencias Nucleares, Universidad Nacional Autónoma de México, Apartado Postal 70-543, México Distrito Federal 04510, México*

E-mail: grigorios.chachamis@csic.es, michal.deak@ific.uv.es, martin.hentschinski@gmail.com, german.rodrigo@csic.es, a.sabio.vera@gmail.com

Abstract: We present a study within the k_T-factorisation scheme on single bottom quark production at the LHC. In particular, we calculate the rapidity and transverse momentum differential distributions for single bottom quark/anti-quark production. In our setup, the unintegrated gluon density is obtained from the NLx BFKL Green function whereas we included mass effects to the Lx heavy quark jet vertex. We compare our results to the corresponding distributions predicted by the usual collinear factorisation scheme. The latter were produced with Pythia 8.1.

Contents

1 Introduction

Major theoretical developments in the last three decades in small-x physics made possible phenomenological analyses of high energy scattering processes within the k_T-factorization scheme [1–3] at ep (HERA) and hadron colliders (Tevatron, LHC). The Balitsky-Fadin-Kuraev-Lipatov (BFKL) framework for the resummation of high center-of-mass energy logarithms at leading (LL) [4] and next-to-leading (NLL) [5] logarithmic accuracy is in the core of the majority of these analyses.

It is very natural to wonder whether the knowledge acquired from the study of Deep Inelastic Scattering (DIS) processes at HERA within the BFKL formalism, mainly from the description of F_2 and F_L data, could be of direct use for the description of processes at the LHC. In principle, factorization and universality dictate the existence of a transition approach from ep to hadron-hadron collisions [6–8], despite the different kinematic phase space limits. A simple way for that to be realized and act as a proof of concept is to use an unintegrated gluon density from HERA fits into a phenomenological study of an LHC process. Recently, there were successful attempts for the detailed description of the Q^2 and x dependence of the structure functions F_2 and F_L by making use of a collinearly-improved BFKL equation at next-to-leading logarithmic (NLx) accuracy [9, 10].[1]

Within high energy factorization, the description of any hard process requires three ingredients: the universal BFKL gluon Green's function which resums high energy logarithms and two process dependent impact factors which describe the coupling of scattering particles to the gluon Green's function. In the present case, only one impact factor (the 'heavy quark impact factor') is characterized by a hard scale *i.e.* the heavy quark mass and large transverse momentum which enables us to calculated it using perturbative QCD and collinear factorization. The second impact factor (the 'proton impact factor'), which describes the coupling of the gluon Green's function to the proton, is intrinsically non-perturbative and needs to be modeled. Combination of the gluon Green's function and the proton impact

[1] See also the works in Refs. [11, 12].

factor yields then the above mentioned unintegrated gluon density. The impact factors for gluons and massless quarks have been calculated in Ref. [13–15], at NLx. The NLx impact factor for a massive quark in the initial state has been calculated in Ref. [16, 17].

In the last years, studies of BFKL evolution were mainly focused on processes with two hard scales of similar sizes in the final state to suppress any collinear-like evolution, with Mueller-Navelet jets [8] the best known example. Most of the studies were carried out at NLx accuracy [6, 18–25].

On the other hand there has been also considerable interest in the study of processes with one hard scale, which involve unintegrated or Transverse Momentum Dependent (TMD) parton density functions (PDFs). Examples of such processes at the LHC include forward jet [26–29] and forward Z production [30, 31]. During recent years the study of TMD PDFs has become a very active area of research, which find applications in various multi-scale processes in hadronic collisions, see Ref. [32] for a recent review. Extraction of TMD PDFs has in some cases been developed to very sophisticated levels, including a detailed discussion of experimental uncertainties, see *e.g.* [33].

In this paper, we study single bottom (or anti-bottom) quark production at the LHC. Bottom quark production (more accurately, bottom pair production) has received lots of attention in the literature [34–45] both in the collinear and the k_T-factorization approach. Bottom quarks can generally be produced via gluon splitting, $g \to b\overline{b}$ in proton-proton collisions. Since our main purpose here is to test the unintegrated gluon density from the HERA fit [9, 10] and to compare it to theoretical predictions from collinear factorization at small x, we concentrate in the following on bottom quark production in the forward region of one of the protons. In this way the heavy quark – as an incoming parton – will be fixed at relatively large x, while the second parton – a gluon – is forced into the small-x region. Measurement of such a process will be possible within the LHCb experiment [57] and currently discussed forward updates of the ATLAS and CMS experiments.

While the unintegrated gluon density extracted from [9, 10] does not provide a detailed discussion of experimental uncertainties (unlike *e.g.* [33]), it is the only currently available unintegrated gluon density which is subject to BFKL evolution at NLL accuracy, including a resummation of large logarithms at the level of the next-to-leading order BFKL kernel. In this sense the current studies present an advance over previous attempts based on LL accuracy.

The article is structured as follows: in Section 2 we introduce the high energy factorization framework we will use and in Section 3 we derive the master formula for the differential single bottom quark cross-section. In Section 4 we present the numerical results and we conclude in Section 5.

2 Forward single bottom quark production in high energy factorization

In the following we will study for typical LHC center-mass-energies $\sqrt{s} = 8$ and 13 TeV the process

$$\text{proton}(p_1) + \text{proton}(p_2) \to \text{bottom quark jet}(k) + X \tag{2.1}$$

where the jet rapidity is assumed to be close to the forward region of the scattering proton with momentum p_1. We assume in the following light-like proton momenta p_1 and p_2, with $2p_1 \cdot p_2 = s$. For the above process, the bottom quark jet provides a hard scale, both through the bottom mass m_b and its transverse momentum k_T, which allows for an an analysis of this process within QCD perturbation theory. Furthermore, since the scattering proton with momentum p_2 is separated from both the heavy quark jet and the proton with momentum p_1 by a large interval in rapidity, a description of the process within high energy factorization is possible. For sufficiently high k_T, this process is then described at leading order through the partonic process $Q + g \to Q'$ convoluted with corresponding gluon and heavy quark distribution functions. Within high energy factorization, the initial heavy quark is always taken at large $x_Q \sim 1$, while the gluon is pushed into the small $x_g \ll 1$ region, with the opposite configuration ($x_Q \ll 1$ and $x_g \sim 1$) suppressed by powers of the center-of-mass energy. For the further analysis within high energy factorization (which includes a resummation a large terms $(\alpha_s \ln 1/x_g)^n \sim 1$ to all orders in α_s), it is then sufficient to analyze the process

$$Q(x_Q \cdot p_1) + p(p_2) \to \text{bottom quark jet}(k) + X', \tag{2.2}$$

i.e. we study scattering of a heavy quark on a proton together with production of a heavy quark jet in high energy limit, see Fig. 1. The cross-section for for this process σ_Q can be written as a convolution of three objects: the partonic heavy quark impact factor, the gluon Green's function, which is a process independent universal quantity and the proton impact factor. Formally, this means that we can write for the forward bottom quark cross-section:

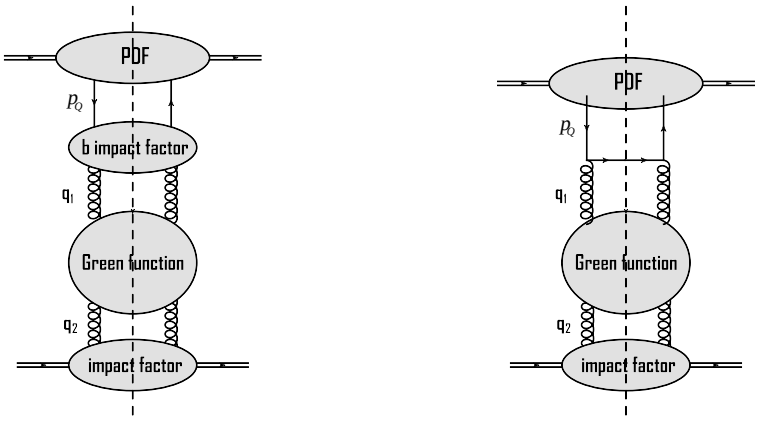

Figure 1. Single bottom quark production in high energy factorization. The cross-section is given by a convolution of the gluon Green's function, the proton impact factor (at the bottom of the diagram) and the bottom quark impact factor. A generic order heavy quark impact factor is depicted to the left whereas to the right the Lx impact factor is shown.

$$\sigma_Q(x_g, Q^2) = \frac{1}{(4\pi)^4} \int \frac{d^2\boldsymbol{q}_1}{\boldsymbol{q}_1^2} \int \frac{d^2\boldsymbol{q}_2}{\boldsymbol{q}_2^2} \Phi_Q(q_1, Q^2) \mathcal{F}^{\text{DIS}}(x, q_1, q_2) \Phi_p(q_2, Q_0^2), \tag{2.3}$$

where Q is the hard scale related to the final state heavy quark momentum. We have introduced $q_i = \sqrt{\boldsymbol{q}_i^2}$, $i = 1, 2$ (the transverse momenta of t-channel gluons, see Fig. 1). In the equation (2.3) $\Phi_Q(q_1, Q^2)$ is the heavy quark impact factor, $\Phi_p(q_2, Q_0^2)$ the proton impact factor and $\mathcal{F}^{\rm DIS}(x, q_1, q_2)$ the gluon Green's function adapted for DIS-like kinematics. $\Phi_Q(q_1, Q^2)$ and $\mathcal{F}^{\rm DIS}(x, q_1, q_2)$ are quantities, that are calculable in perturbative QCD whereas $\Phi_p(q_2, Q_0^2)$ is an object of intrinsic non-perturbative nature and has to be modeled. We will use in this study the fit of Refs. [9, 10] which achieves a successful description of F_2 and F_L HERA data with a very simple ansatz for the proton impact factor with three independent parameters.

When the two scales Q^2 and Q_0^2 are similar in size, the gluon Green's function $\mathcal{F}$ – which is obtained as the solution to the BFKL equation – can be written at leading order as

$$\mathcal{F}^{\rm Lx}(s, q_1, q_2) = \frac{1}{2\pi q_1\, q_2} \int \frac{d\omega}{2\pi i} \int \frac{d\gamma}{2\pi i} \left(\frac{q_1^2}{q_2^2}\right)^{\gamma - \frac{1}{2}} \left(\frac{s}{q_1\, q_2}\right)^{\omega} \frac{1}{\omega - \bar{\alpha}_s \chi_0(\gamma)}, \tag{2.4}$$

with $\bar{\alpha}_s = \alpha_s N_c/\pi$ and $\chi_0(\gamma) = 2\psi(1) - \psi(\gamma) - \psi(1-\gamma)$ the eigenvalue of the Lx BFKL kernel with $\psi(\gamma)$ is the logarithmic derivative of the Euler Gamma function. The gluon Green's function is universal and resums $\bar{\alpha}_s^n \log^n s$ terms to all-orders in the strong coupling.

In our setup however, $Q^2 \gg Q_0^2$ and this expression should be written in a form consistent with the resummation of $\bar{\alpha}_s \log(1/x)$ contributions:

$$\mathcal{F}(s, q_1, q_2) = \frac{1}{2\pi q_1^2} \int \frac{d\omega}{2\pi i} \int \frac{d\gamma}{2\pi i} \left(\frac{q_1^2}{q_2^2}\right)^{\gamma} \left(\frac{s}{q_1^2}\right)^{\omega} \frac{1}{\omega - \bar{\alpha}_s \chi_0\left(\gamma - \frac{\omega}{2}\right)}. \tag{2.5}$$

In the limits $\gamma \to 0, 1$, the zeros of the denominator of the integrand generate all-orders terms not compatible with DGLAP evolution [46, 47]. By taking into account the NLx correction to the BFKL kernel, the first of these pieces ($\mathcal{O}(\alpha_s^2)$) is removed. Higher orders though however remain and are numerically important. A scheme to eliminate these spurious contributions was introduced in [46] by using a modified BFKL kernel in Eq. (2.4) incorporating the change $\chi_0(\gamma) \to 2\psi(1) - \psi(\gamma + \frac{\omega}{2}) - \psi(1 - \gamma + \frac{\omega}{2})$.

The NLx kernel after collinear improvements can very well be approximated by breaking the transcendentality of the NLx kernel and solving it pole by pole and summing up the different solutions. This procedure was introduced in Ref. [47] and we refer the reader there for further details. The NLx kernel with collinear improvements we will be using hereafter reads

$$\chi(\gamma) = \bar{\alpha}_s \chi_0(\gamma) + \bar{\alpha}_s^2 \chi_1(\gamma) - \frac{1}{2}\bar{\alpha}_s^2 \chi_0'(\gamma)\, \chi_0(\gamma) + \chi_{RG}(\bar{\alpha}_s, \gamma, a, b). \tag{2.6}$$

with

$$\begin{aligned} \chi_{RG}(\bar{\alpha}_s, \gamma, a, b) \;=\; & \bar{\alpha}_s(1 + a\bar{\alpha}_s)\left(\psi(\gamma) - \psi(\gamma - b\bar{\alpha}_s)\right) \\ & - \frac{\bar{\alpha}_s^2}{2}\psi''(1-\gamma) - b\bar{\alpha}_s^2 \frac{\pi^2}{\sin^2(\pi\gamma)} + \frac{1}{2}\sum_{m=0}^{\infty}\Bigg(\gamma - 1 - m + b\bar{\alpha}_s \\ & - \frac{2\bar{\alpha}_s(1 + a\bar{\alpha}_s)}{1 - \gamma + m} + \sqrt{(\gamma - 1 - m + b\bar{\alpha}_s)^2 + 4\bar{\alpha}_s(1 + a\bar{\alpha}_s)}\Bigg). \end{aligned} \tag{2.7}$$

For the NLx BFKL kernel we have:

$$\chi_1(\gamma) = \mathcal{S}\chi_0(\gamma) - \frac{\beta_0}{8N_c}\chi_0^2(\gamma) + \frac{\Psi''(\gamma)+\Psi''(1-\gamma)-\phi(\gamma)-\phi(1-\gamma)}{4} - \frac{\pi^2\cos(\pi\gamma)}{4\sin^2(\pi\gamma)(1-2\gamma)}\left[3+\left(1+\frac{n_f}{N_c^3}\right)\frac{2+3\gamma(1-\gamma)}{(3-2\gamma)(1+2\gamma)}\right] + \frac{3}{2}\zeta(3), \tag{2.8}$$

with $\mathcal{S} = \frac{1}{3} - \frac{\pi^2}{12} + \frac{5\beta_0}{12N_c}$, $\beta_0 = \left(\frac{11}{3}N_c - \frac{2}{3}n_f\right)$ and

$$\phi(\gamma)+\phi(1-\gamma) = \sum_{m=0}^{\infty}\left(\frac{1}{\gamma+m}+\frac{1}{1-\gamma+m}\right)\left[\Psi'\left(1+\frac{m}{2}\right)-\Psi'\left(\frac{1+m}{2}\right)\right], \tag{2.9}$$

whereas the coefficients a and b read

$$a = \frac{5}{12}\frac{\beta_0}{N_c} - \frac{13}{36}\frac{n_f}{N_c^3} - \frac{55}{36}, \qquad b = -\frac{1}{8}\frac{\beta_0}{N_c} - \frac{n_f}{6N_c^3} - \frac{11}{12}. \tag{2.10}$$

To achieve a model with sensible parameters for the proton impact factor dominated by the infrared region, the Brodsky-Lepage-Mackenzie (BLM) optimal scale setting scheme [48] has been used in [9, 10] to fix the renormalization scale.[2] The BLM procedure is a way of absorbing the non conformal terms of the perturbative series in a redefinition of the coupling constant, to improve the convergence of the perturbative series. Practically, one needs to extract the β_0-dependent part of an observable and choose the renormalization scale such that this part vanishes. In the current case this leads to

$$\tilde{\alpha}_s(QQ_0,\gamma) = \frac{4N_c}{\beta_0\left[\log\left(\frac{QQ_0}{\Lambda^2}\right)+\frac{1}{2}\chi_0(\gamma)-\frac{5}{3}+2\left(1+\frac{2}{3}Y\right)\right]}, \tag{2.11}$$

where we are using the momentum space (MOM) physical renormalization scheme based on a symmetric triple gluon vertex [52] with $Y \simeq 2.343907$ and gauge parameter $\xi = 3$ The modifications we need in the BFKL kernel in order to introduce this new scheme are $\bar{\alpha}_s \to \tilde{\alpha}_s(QQ_0,\gamma)$ and $\chi_1(\gamma) \to \tilde{\chi}_1(\gamma)$ in Eqs. (2.6), (2.8) together with the corresponding adjustments for the coefficients $a, b \to \tilde{a}, \tilde{b}$ which enter Eq. (2.7). The modified quantities read

$$\tilde{\chi}_1(\gamma) = \tilde{\mathcal{S}}\chi_0(\gamma) + \frac{3}{2}\zeta(3) + \frac{\Psi''(\gamma)+\Psi''(1-\gamma)-\phi(\gamma)-\phi(1-\gamma)}{4} - \frac{\pi^2\cos(\pi\gamma)}{4\sin^2(\pi\gamma)(1-2\gamma)}\left[3+\left(1+\frac{n_f}{N_c^3}\right)\frac{2+3\gamma(1-\gamma)}{(3-2\gamma)(1+2\gamma)}\right] + \frac{1}{8}\left[\frac{3}{2}(Y-1)\xi + \left(1-\frac{Y}{3}\right)\xi^2 + \frac{17Y}{2} - \frac{\xi^3}{6}\right]\chi_0(\gamma), \tag{2.12}$$

$$\tilde{a} = -\frac{13}{36}\frac{n_f}{N_c^3} - \frac{55}{36} + \frac{3Y-3}{16}\xi + \frac{3-Y}{24}\xi^2 - \frac{1}{48}\xi^3 + \frac{17}{16}Y \tag{2.13}$$

$$\tilde{b} = -\frac{n_f}{6N_c^3} - \frac{11}{12}, \tag{2.14}$$

[2] The first application of the BLM scheme was in Ref. [49–51] in the context of virtual photon-photon scattering.

where $\tilde{\mathcal{S}} = \frac{(4-\pi^2)}{12}$. In addition, in order to access the region of small photon virtualities, in [9, 10], a parametrization of the running coupling introduced by Webber in Ref. [53] has been used,

$$\alpha_s\left(\mu^2\right) = \frac{4\pi}{\beta_0 \ln \frac{\mu^2}{\Lambda^2}} + f\left(\frac{\mu^2}{\Lambda^2}\right), \quad f\left(\frac{\mu^2}{\Lambda^2}\right) = \frac{4\pi}{\beta_0} \frac{125\left(1+4\frac{\mu^2}{\Lambda^2}\right)}{\left(1-\frac{\mu^2}{\Lambda^2}\right)\left(4+\frac{\mu^2}{\Lambda^2}\right)^4}, \tag{2.15}$$

with $\Lambda = 0.21$ GeV. At low scales this modified running coupling is consistent with global data of power corrections to perturbative observables, while for larger values it coincides with the conventional perturbative running coupling constant.

Let us add here, that in a future analysis we plan to investigate effects related to the choice of the renormalization scale and the choice of the parametrization of the running of the strong coupling (see Ref. [17] and also Refs. [54–56]).

3 The differential cross-section with bottom mass effects included

As already mentioned in the previous section, the non-perturbative proton impact factor has to be modeled. We use here the same functional form as in Refs. [9, 10]:

$$\Phi_p\left(q, Q_0^2\right) = \frac{\mathcal{C}}{2\pi\Gamma\left(\delta\right)} \left(\frac{q^2}{Q_0^2}\right)^{\delta} e^{-\frac{q^2}{Q_0^2}}, \tag{3.1}$$

which introduces three independent free parameters and has a maximum at $q^2 = \delta\, Q_0^2$. Its representation in γ space reads

$$h_p(\gamma) = \int \frac{d^2\boldsymbol{q}}{\pi} \Phi_p\left(q, Q_0^2\right) \left(q^2\right)^{-\gamma-1} = \mathcal{C}\, \frac{\Gamma(\delta-\gamma)}{2\pi\Gamma\left(\delta\right)} (Q_0^2)^{-\gamma}. \tag{3.2}$$

The values of the parameters Q_0, δ and $\mathcal{C}$ were determined from a fit to combined HERA data. When the leading order photon impact factor was used the obtained values were $Q_0 = 0.28$ GeV, $\delta = 8.4$ and $\mathcal{C} = 1.50$ whereas in the case of the kinematically improved photon impact factor the last two change to $\mathcal{C} = 2.35$ and $\delta = 6.5$ with the number of flavors fixed to $n_f = 4$. We use both sets of values for $\mathcal{C}$ and δ in our numerical study later. Combining the BFKL Green's function for DIS kinematics and the proton impact factor, we obtain the following expression for an unintegrated gluon density within our setup

$$G(x, q_1) = \int \frac{d\boldsymbol{q}_2^2}{\boldsymbol{q}_2^2} \mathcal{F}^{\mathrm{DIS}}\left(x, q_1, q_2\right) \Phi_p\left(q_2, Q_0^2\right) \ . \tag{3.3}$$

To obtain the complete NLx BFKL Green's function we need to add to Eq. (2.4) apart from the NLx correction to the BFKL eigenvalue, non-exponentiating NLx β_0 terms. Following the treatment of Ref.[10] one obtains

$$\begin{aligned} G\left(x, q_1, Q\right) = \frac{1}{q_1^2} \int_{-\infty}^{\infty} \frac{d\nu}{2\pi^2} \ \frac{\mathcal{C}\cdot\Gamma(\delta - i\nu - \frac{1}{2})}{\Gamma(\delta)} \ \cdot \left(\frac{1}{x}\right)^{\chi\left(\frac{1}{2}+i\nu\right)} \left(\frac{q_1^2}{Q_0^2}\right)^{\frac{1}{2}+i\nu} \times \\ \left\{1 + \frac{\bar{\alpha}_s^2 \beta_0 \chi_0\left(\frac{1}{2}+i\nu\right)}{8N_c} \log\left(\frac{1}{x}\right) \left[-\psi\left(\delta - \frac{1}{2} - i\nu\right) - \log\frac{q_1^2}{Q^2}\right]\right\}. \end{aligned} \tag{3.4}$$

In the DIS analysis Q^2 has been identified with the virtuality of the photon. In the present study we use instead the transverse momentum of the bottom quark, $Q = k_T$, with $k_T = \sqrt{\boldsymbol{k}^2}$ the modulus of the transverse momentum of the heavy quark. The other obvious choice for $Q = \sqrt{k_T^2 + m_b^2}$ causes only small differences in the results.

Once we have the formal definition of the gluon density given by Eqs. (3.3) and (3.4), we can have an alternative view at Qp-scattering depicted in Fig. 1. In particular, we may consider it as a convolution of the bottom quark impact factor with the gluon density as shown in Fig. 2. To obtain the complete forward heavy quark cross-section, we further

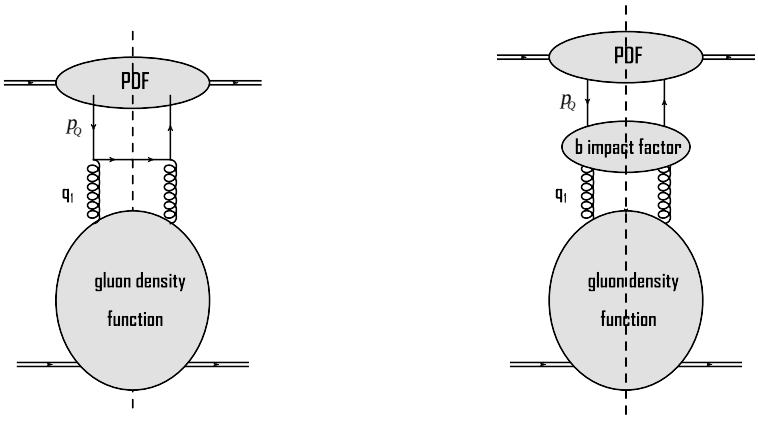

Figure 2. The same process as in Fig. 1 here presented as a convolution of the bottom quark impact factor and the gluon density.

require the bottom quark jet vertex which at leading order coincides with the massless quark impact factor modulo Dirac Delta functions to ensure momentum conservation. The heavy quark jet vertex at Lx depends therefore only implicitly on the quark mass through the final state phase-space integration. We should stress here, that a proper NLx study with mass effects properly introduced would be the desirable goal. Currently only the inclusive heavy quark impact factor, which describes the process $Q + g^* \to X''$, is available at NLx accuracy [16, 17]. While at leading order inclusive and jet impact factor coincide, a NLx description of the process $Q + g^* \to$ bottom quark jet $+ X'''$ will depend explicitly on the details of the employed jet algorithm and hence differs from the corresponding inclusive result. In the current study we therefore restrict ourselves to the Lx jet vertex. The leading order impact factor is then obtained from the squared amplitude of the subprocess $Q + g^* \to Q'$, integrated over the one-particle invariant phase space $d\Phi^{(1)}$. The momenta of the incoming quark and gluon can be expressed in Sudakov variables as $p_Q = x_Q p_1$ and $p_g = x_g p_2 + \boldsymbol{q}_1$ respectively. Energy-momentum conservation identifies then the gluon transverse momentum with the transverse momentum of the final state bottom quark $\boldsymbol{q}_1 = \boldsymbol{k}$; the one-particle phase space of the heavy quarks reads $d\Phi^{(1)} = 2\pi\delta(x_Q x_g s - \boldsymbol{k}^2 - m_b^2)$. After a bit of Algebra, we obtain for the $Q + g^* \to Q'$ partonic cross-section:

$$\hat{\sigma} = \sigma_0 \delta(x_Q x_g s - \boldsymbol{k}^2 - m_b^2) \,, \qquad \sigma_0 = \frac{\alpha_s 2\pi^2}{N_c} \,.$$

The total $pp \to Q + X$ cross-section then reads

$$\sigma_{pp\to Q+X} = \int_0^1 dx_Q \int_0^1 \frac{dx_g}{x_g} \int \frac{d^2\boldsymbol{k}}{\pi} \hat{\sigma} \cdot \left[f_Q(x_Q, \mu_f) + f_{\bar{Q}}(x_Q, \mu_f) \right] G(x_g, \boldsymbol{k}_T, Q) \,. \tag{3.5}$$

with f_i, $i = Q, \bar{Q}$ the collinear (anti-) bottom quark distribution and μ_f the collinear factorization scale. Fixing $x_g = (\boldsymbol{k}^2 + m_b^2)/x_Q s$ and introducing the rapidity of the produced bottom quark $\eta = \frac{1}{2} \ln \frac{x_Q}{x_g}$, the total cross-section is recast into

$$\begin{aligned} \sigma_{pp\to Q+X} &= \int_{-\infty}^{\infty} d\eta \int \frac{d^2\boldsymbol{k}}{\pi} \frac{\sigma_0}{x_Q x_g s} \, x_Q \left[f_Q(x_Q, \mu_f) + f_{\bar{Q}}(x_Q, \mu_f) \right]) \, G(x_g, k_T, Q) \\ &= \int_{-\infty}^{\infty} d\eta \int \frac{d^2\boldsymbol{k}}{\pi} \frac{\sigma_0}{k_T^2 + m_b^2} \, x_Q \left[f_Q(x_Q, \mu_f) + f_{\bar{Q}}(x_Q, \mu_f) \right] \, G(x_g, k_T, Q) \,. \end{aligned} \tag{3.6}$$

After integrating over the azimuthal angle of $\boldsymbol{k}$, the $pp \to Q' + X$ double differential cross-section finally reads

$$\frac{d\sigma_{pp\to Q+X}}{d\eta \, dk_T} = \frac{2k_T \cdot \sigma_0}{k_T^2 + m_b^2} \, x_Q \, \left[f_Q(x_Q, \mu_f) + f_{\bar{Q}}(x_Q, \mu_f) \right] \, G(x_g, k_T^2, Q) \,. \tag{3.7}$$

with

$$x_Q = e^{\eta} \sqrt{\frac{m_b^2 + \boldsymbol{k}^2}{s}} \,, \qquad x_g = e^{-\eta} \sqrt{\frac{m_b^2 + \boldsymbol{k}^2}{s}} \,. \tag{3.8}$$

Leaving aside for the time being the dependence on the collinear bottom quark distribution function $x_Q \, f_i(x_Q)$, $i = Q, \bar{Q}$ we will have for the $Qp \to Q'$ cross-section in ν-space

$$\begin{aligned} \frac{d\sigma_{Qp\to Q'}}{d\eta dk_T} = \; & \frac{\sigma_0 \cdot \mathcal{C}}{k_T \cdot (k_T^2 + m_b^2)} \int_{-\infty}^{\infty} \frac{d\nu}{\pi^2} \, x^{-\chi(\frac{1}{2}+i\nu)} \, \frac{\Gamma\left(\delta - \frac{1}{2} - i\nu\right)}{\Gamma(\delta)} \, \left(\frac{k_T^2}{Q_0^2} \right)^{1/2+i\nu} \\ & \times \left\{ 1 + \bar{\alpha}_s^2 \log\left(\frac{1}{x}\right) \frac{\beta_0}{8N_c} \chi_0\left(\frac{1}{2} + i\nu\right) \left[-\psi^{(0)}\left(\delta - i\nu - \frac{1}{2}\right) \right] \right\} \,. \end{aligned} \tag{3.9}$$

Fixing the factorization scale of the bottom quark PDF to $\mu_f = \sqrt{k_T^2 + m_b^2}$, the double differential cross-section for single bottom quark production in proton-proton collisions reads

$$\frac{d\sigma_{pp\to Q'+X}}{d\eta \, dk_T} = \frac{d\sigma_{Qp\to Q'}}{d\eta \, dk_T} \, x_Q \left[f_Q\left(x_Q, \sqrt{k_T^2 + m_b^2}\right) + f_{\bar{Q}}\left(x_Q, \sqrt{k_T^2 + m_b^2}\right) \right] \,, \tag{3.10}$$

which we use to produce all of our numerical results in the next section.

4 Numerical results

In this section we present our predictions for the differential cross-section, η- and k_T-distribution, for single bottom quark/anti-quark production at the LHC. The analysis does not make distinction between the bottom quark and anti-quark.

In Fig. 3, we show the range of maximal/minimal x_g for each value of k_T. The light blue area corresponds to the Bjorken x and Q ranges of the data, that were used for the F_2 and F_L fit in [9, 10]. The light orange area corresponds to the x_g and k_T ranges in our calculation of the bottom quark cross-section when the rapidity takes values between 1 and 5 and k_T is constrained to 4 GeV$< k_T <$ 100 GeV. Lastly, the light red area corresponds to the x and k_T ranges when the rapidity takes values between 3 and 5 and k_T is constrained to 4 GeV$< k_T <$ 50 GeV. This kinematical range is not covered by the general purpose detectors ATLAS and CMS, but is accessible by the LHCb detector [57] designed for these kind of measurements.

It is more than evident, that the kinematic region we are covering for bottom quark production does not overlap at all with the kinematic region in which the unintegrated gluon density was obtained. In particular, the values of the unintegrated gluon density tested in our setup are not directly constrained by HERA data. They are rather calculated through evolving the results of the HERA fit towards both smaller x values and larger k_T using our collinear improved solution to the BFKL equation. Nevertheless, as we shall see, the unintegrated gluon density based on that specific model, gives results very close to PYTHIA 8.1. It has to be stressed though, that the whole approach carries uncertainties which at present cannot be quantified and one has to be cautious not to interpret these high energy factorization results as the final word within the BFKL approach.

In all the next figures, predictions with $\delta = 8.4$ and $\mathcal{C} = 1.5$ are plotted with solid red lines, the results with $\delta = 6.5$ and $\mathcal{C} = 2.35$ are plotted with dashed red lines and the results by PYTHIA 8.1 are plotted with purple solid lines. We have used the MSTW 2008 NLO parton density functions [58] throughout the entire section. The bottom quark mass was set to $m_b = 4.7$ GeV for the high energy factorization result whereas in PYTHIA 8.1 the program default value was used.

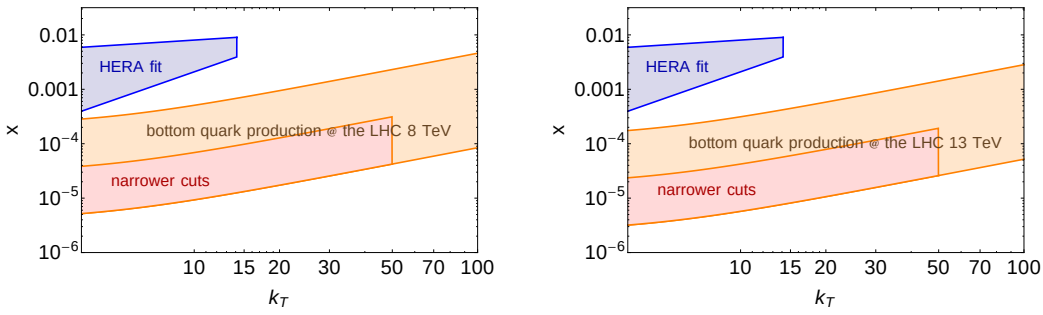

Figure 3. Light blue area: kinematic region corresponding to the original fit of the proton impact factor. Light orange area: phase space for the kinematic cuts ($1 < \eta < 5$, 4 GeV$< k_T <$ 100 GeV). Light red area: phase space for the kinematic cuts ($3 < \eta < 5$, 4 GeV$< k_T <$ 50 GeV).

In Figs. 4 and 5 we present results for $\sqrt{s} = 8$ TeV and in Figs. 6 and 7 for $\sqrt{s} = 13$ TeV. In Figs. 4 and 6 we integrate the differential cross-section (3.10) over the rapidity of the quark in the range $1 < \eta < 5$ and over k_T in the range 4 GeV $< k_T <$ 100 GeV while in Figs. 5 and 7 we integrate over the rapidity of the quark in the range $3 < \eta < 5$ and over the transverse momentum in the range 4 GeV $< k_T <$ 50 GeV. The differential distributions are

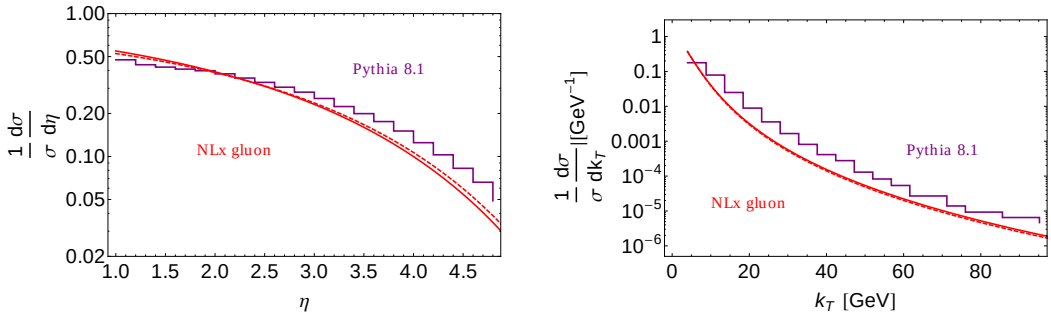

Figure 4. Collision energy $\sqrt{s} = 8$ TeV. Left: η-distribution after integrating over k_T in the range 4 GeV $< k_T <$ 100 GeV. Right: k_T-distribution after integrating over η in the range $1 < \eta < 5$. Both distributions are normalized by the integrated cross-section over η and k_T in the ranges 4 GeV $< k_T <$ 100 GeV and $1 < \eta < 5$.

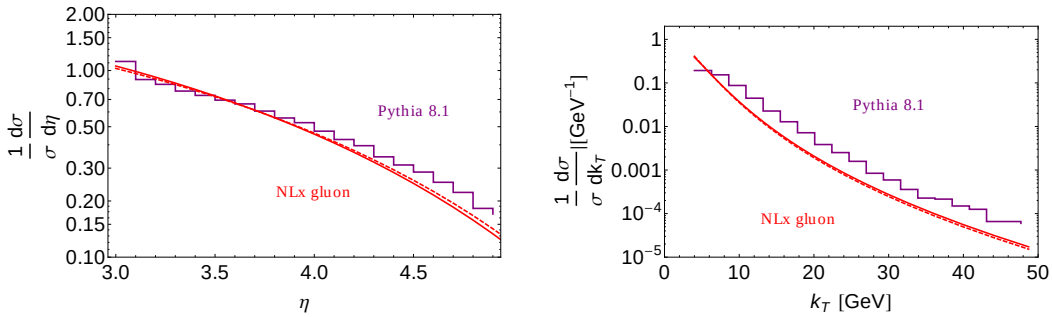

Figure 5. Collision energy $\sqrt{s} = 8$ TeV. Left: η-distribution after integrating over k_T in the range 4 GeV $< k_T <$ 50 GeV. Right: k_T-distribution after integrating over η in the range $3 < \eta < 5$. Both distributions are normalized by the integrated cross-section over η and k_T in the ranges 4 GeV $< k_T <$ 50 GeV and $3 < \eta < 5$.

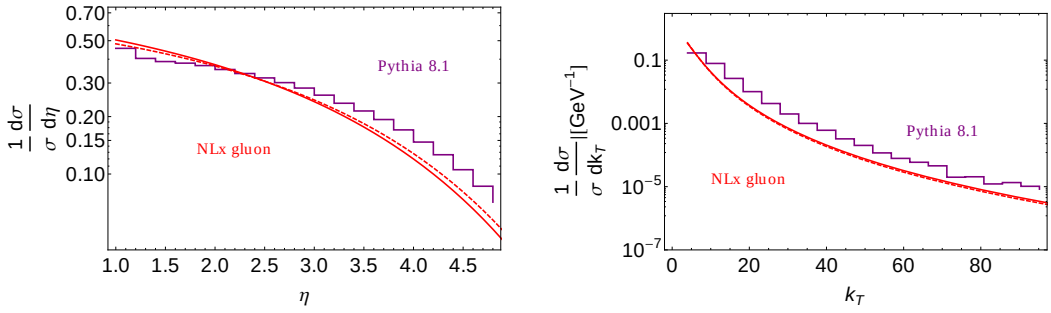

Figure 6. Collision energy $\sqrt{s} = 13$ TeV. Left: η-distribution after integrating over k_T in the range 4 GeV $< k_T <$ 100 GeV. Right: k_T-distribution after integrating over η in the range $1 < \eta < 5$. Both distributions are normalized by the integrated cross-section over η and k_T in the ranges 4 GeV $< k_T <$ 100 GeV and $1 < \eta < 5$.

normalized by the integrated cross-section over the corresponding rapidity and k_T ranges.

A first observation is that when we compare the k_T distributions calculated in high energy factorization and by PYTHIA 8.1 we see the former to be smaller than the latter due to the difference in the shape at small k_T. The shape of the k_T distribution though is very

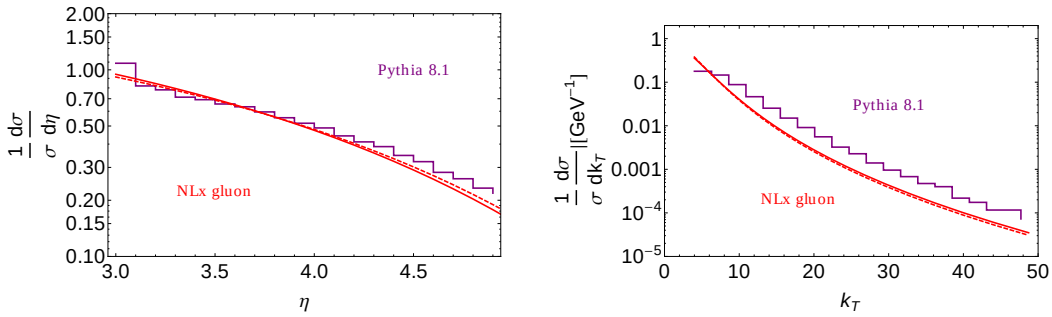

Figure 7. Collision energy $\sqrt{s} = 13$ TeV. Left: η-distribution after integrating over k_T in the range 4 GeV $< k_T <$ 50 GeV. Right: k_T-distribution after integrating over η in the range $3 < \eta < 5$. Both distributions are normalized by the integrated cross-section over η and k_T in the ranges 4 GeV $< k_T <$ 50 GeV and $3 < \eta < 5$.

similar at large k_T in both approaches.

The main finding comes forward when we focus on the rapidity distributions. The high energy factorization result seems to be somehow larger than the PYTHIA 8.1 estimate for small rapidities whereas for larger η it drops faster than the PYTHIA 8.1 result and at the high end of the rapidity it lies below it. The same trend is followed for both center-of-mass energies and for both k_T integration ranges (4 GeV $< k_T <$ 50 GeV and 4 GeV $< k_T <$ 100 GeV).

Finally, let us note, that a change of values for the parameters δ and $\mathcal{C}$ from $\delta = 8.4$ and $\mathcal{C} = 1.5$ to $\delta = 6.5$ and $\mathcal{C} = 2.35$ results to a slightly smaller NLx cross-section.

5 Conclusions and Outlook

We have presented a study of the rapidity and k_T (transversal momentum) differential distributions for single bottom quark production at the LHC calculated both in high energy factorization and by the Monte Carlo program PYTHIA 8.1. and for $\sqrt{s} = 8$ and 13 TeV. Within the former framework, we have used a model for the proton impact factor, the NLx BFKL gluon Green's function and the Lx heavy quark jet vertex with bottom mass effects included.

The main result of our study concerns the rapidity distributions. The high energy factorization estimate is for small rapidities larger than the PYTHIA 8.1 result but as the rapidity approaches some middle range value, the fall becomes steeper and the estimate gets smaller than the PYTHIA 8.1 estimate. The k_T-distributions have very similar shapes but the PYTHIA 8.1 result is almost always larger.

The calculation presented in this article suggests, within its limitations, namely, that it is only a partial NLx calculation and that the unintegrated gluon density is probed in a region not covered by the F_2 and F_L fit, that single bottom quark production might be used as an experimental probe of the k_T-factorization scheme and the validity of high energy factorization for LHC processes. It also shows, that our initial assumption, that the unintegrated gluon density from HERA would not fail at the LHC, was justified. We plan to extend our study toward obtaining more exclusive information with regard to the final state

by using the BFKL Monte Carlo code BFKLex [59, 60]. The code is an implementation of an iterative solution to the NLx BFKL equation and has already been used in a number of projects [61–63]. We expect, that once the NLx massive quark jet vertex is ready, we will able to present a more refined study of the process and a detailed analysis on the BFKL predictions for the single bottom quark cross section.

Acknowledgements

M. D. acknowledges support from Juan de la Cierva programme (JCI-2011-11382). M. H. acknowledges support by UNAM-DGAPA-PAPIIT grant number 101515 and CONACyT-Mexico grant number 128534. G. C. acknowledges support from Marie Curie Actions (PIEF-GA-2011-298582). A.S.V. acknowledges support from European Commission under contract LHCPhenoNet (PITN-GA-2010-264564), Madrid Regional Government (HEPHACOSESP-1473), Spanish Government (MICINN (FPA2010-17747)) and Spanish MINECO Centro de Excelencia Severo Ochoa Programme (SEV-2012-0249). This work has been supported in part by the Spanish Government and ERDF funds from the EU Commission [Grants No. FPA2011-23778, FPA2014-53631-C2-1-P No. CSD2007-00042 (Consolider Project CPAN)] and by Generalitat Valenciana under Grant No. PROMETEOII/2013/007. This work has been supported in part by the Ministry of Economy and Competitiveness (MINECO), under grant number FPA2013-44773-P

References

[1] S. Catani, M. Ciafaloni and F. Hautmann, Phys. Lett. B **242**, 97 (1990).

[2] S. Catani, M. Ciafaloni and F. Hautmann, Nucl. Phys. B **366**, 135 (1991).

[3] S. Catani and F. Hautmann, Nucl. Phys. B **427**, 475 (1994) [hep-ph/9405388].

[4] L. N. Lipatov, Sov. J. Nucl. Phys. **23** (1976) 338; E. A. Kuraev, L. N. Lipatov, V. S. Fadin, Phys. Lett. B **60** (1975) 50, Sov. Phys. JETP **44** (1976) 443, Sov. Phys. JETP **45** (1977) 199; Ia. Ia. Balitsky, L. N. Lipatov, Sov. J. Nucl. Phys. **28** (1978) 822.

[5] V. S. Fadin, L. N. Lipatov, Phys. Lett. B **429** (1998) 127 [hep-ph/9802290]; M. Ciafaloni, G. Camici, Phys. Lett. B **430** (1998) 349 [hep-ph/9803389].

[6] A. Sabio Vera and F. Schwennsen, Nucl. Phys. B **776** (2007) 170 [hep-ph/0702158].

[7] J. Kwiecinski, A. D. Martin, L. Motyka and J. Outhwaite, Phys. Lett. B **514** (2001) 355 [hep-ph/0105039].

[8] A. H. Mueller and H. Navelet, Nucl. Phys. B **282** (1987) 727.

[9] M. Hentschinski, A. Sabio Vera and C. Salas, Phys. Rev. Lett. **110** (2013) 041601 [arXiv:1209.1353 [hep-ph]].

[10] M. Hentschinski, A. Sabio Vera and C. Salas, Phys. Rev. D **87** (2013) 7, 076005 [arXiv:1301.5283 [hep-ph]].

[11] H. Kowalski, L. N. Lipatov, D. A. Ross and G. Watt, Nucl. Phys. A **854**, 45 (2011).

[12] H. Kowalski, L. N. Lipatov, D. A. Ross and G. Watt, Eur. Phys. J. C **70**, 983 (2010) [arXiv:1005.0355 [hep-ph]].

[13] M. Ciafaloni and D. Colferai, Nucl. Phys. B **538**, 187 (1999) [hep-ph/9806350].

[14] M. Hentschinski and A. Sabio Vera, Phys. Rev. D **85**, 056006 (2012) [arXiv:1110.6741 [hep-ph]].

[15] G. Chachamis, M. Hentschinski, J. D. Madrigal Martínez and A. Sabio Vera, Phys. Rev. D **87**, no. 7, 076009 (2013) [arXiv:1212.4992].

[16] M. Ciafaloni and G. Rodrigo, JHEP **0005** (2000) 042 [hep-ph/0004033].

[17] G. Chachamis, M. Deak and G. Rodrigo, JHEP **1312** (2013) 066 [arXiv:1310.6611].

[18] F. Caporale, D. Y. Ivanov, B. Murdaca and A. Papa, Eur. Phys. J. C **74**, 3084 (2014) [arXiv:1407.8431 [hep-ph]].

[19] B. Ducloue, L. Szymanowski and S. Wallon, Phys. Rev. Lett. **112**, 082003 (2014) [arXiv:1309.3229 [hep-ph]].

[20] B. Ducloue, L. Szymanowski and S. Wallon, JHEP **1305**, 096 (2013) [arXiv:1302.7012 [hep-ph]].

[21] F. Caporale, D. Y. Ivanov, B. Murdaca and A. Papa, Nucl. Phys. B **877**, 73 (2013) [arXiv:1211.7225 [hep-ph]].

[22] D. Colferai, F. Schwennsen, L. Szymanowski and S. Wallon, JHEP **1012**, 026 (2010) [arXiv:1002.1365 [hep-ph]].

[23] C. Marquet and C. Royon, Phys. Rev. D **79**, 034028 (2009) [arXiv:0704.3409 [hep-ph]].

[24] M. Angioni, G. Chachamis, J. D. Madrigal and A. Sabio Vera, Phys. Rev. Lett. **107**, 191601 (2011) [arXiv:1106.6172 [hep-th]].

[25] F. Caporale, B. Murdaca, A. Sabio Vera and C. Salas, Nucl. Phys. B **875**, 134 (2013) [arXiv:1305.4620 [hep-ph]].

[26] G. Chachamis, M. Hentschinski, J. D. Madrigal Martínez and A. Sabio Vera, Phys. Part. Nucl. **45**, no. 4, 788 (2014) [arXiv:1211.2050 [hep-ph]].

[27] M. Hentschinski, J. D. Madrigal Martínez, B. Murdaca and A. Sabio Vera, Phys. Lett. B **735**, 168 (2014) [arXiv:1404.2937 [hep-ph]].

[28] M. Deak, F. Hautmann, H. Jung and K. Kutak, JHEP **0909** (2009) 121 [arXiv:0908.0538 [hep-ph]].

[29] M. Deak, F. Hautmann, H. Jung and K. Kutak, Eur. Phys. J. C **72**, 1982 (2012) [arXiv:1112.6354 [hep-ph]].

[30] F. Hautmann, M. Hentschinski and H. Jung, Nucl. Phys. B **865**, 54 (2012) [arXiv:1205.1759 [hep-ph]].

[31] S. Dooling, F. Hautmann and H. Jung, Phys. Lett. B **736**, 293 (2014) [arXiv:1406.2994 [hep-ph]].

[32] R. Angeles-Martinez *et al.*, arXiv:1507.05267 [hep-ph].

[33] S. Alekhin *et al.*, Eur. Phys. J. C **75**, no. 7, 304 (2015) [arXiv:1410.4412 [hep-ph]].

[34] R. Gauld, J. Rojo, L. Rottoli and J. Talbert, arXiv:1506.08025 [hep-ph].

[35] P. Nason, S. Dawson and R. K. Ellis, Nucl. Phys. B **303**, 607 (1988).

[36] E. L. Berger and H. Contopanagos, Phys. Rev. D **57**, 253 (1998) [hep-ph/9706206].

[37] R. Bonciani, A. Ferroglia, T. Gehrmann and C. Studerus, JHEP **0908** (2009) 067 [arXiv:0906.3671 [hep-ph]].

[38] R. Bonciani, A. Ferroglia, T. Gehrmann, A. von Manteuffel and C. Studerus, JHEP **1101** (2011) 102 [arXiv:1011.6661 [hep-ph]].

[39] H. Fujii and K. Watanabe, Nucl. Phys. A **915** (2013) 1 [arXiv:1304.2221 [hep-ph]].

[40] M. Luszczak, W. Schafer and A. Szczurek, Phys. Lett. B **729**, 15 (2014) [arXiv:1305.4727 [hep-ph]].

[41] H. Fujii and K. Watanabe, Nucl. Phys. A **920**, 78 (2013) [arXiv:1308.1258 [hep-ph]].

[42] R. Zhu, P. Sun and F. Yuan, Phys. Lett. B **727**, 474 (2013) [arXiv:1309.0780 [hep-ph]].

[43] R. Bonciani, A. Ferroglia, T. Gehrmann, A. von Manteuffel and C. Studerus, JHEP **1312** (2013) 038 [arXiv:1309.4450 [hep-ph]].

[44] B. Kniehl, Z. Merebashvili, J. G. Korner and M. Rogal, Phys. Rev. D **78** (2008) 094013 [arXiv:0809.3980 [hep-ph]].

[45] E. L. Berger and R. b. Meng, Phys. Rev. D **49** (1994) 3248 [hep-ph/9310341].

[46] G. P. Salam, JHEP **9807** (1998) 019 [hep-ph/9806482].

[47] A. Sabio Vera, Nucl. Phys. B **722** (2005) 65 [hep-ph/0505128].

[48] S. J. Brodsky, G. P. Lepage and P. B. Mackenzie, Phys. Rev. D **28** (1983) 228.

[49] S. J. Brodsky, V. S. Fadin, V. T. Kim, L. N. Lipatov and G. B. Pivovarov, JETP Lett. **70** (1999) 155 [hep-ph/9901229], JETP Lett. **76** (2002) 249 [Pisma Zh. Eksp. Teor. Fiz. **76** (2002) 306] [hep-ph/0207297].

[50] S. J. Brodsky, F. Hautmann and D. E. Soper, short distance pomeron," Phys. Rev. D **56** (1997) 6957 [hep-ph/9706427].

[51] S. J. Brodsky, F. Hautmann and D. E. Soper, Phys. Rev. Lett. **78** (1997) 803 [Phys. Rev. Lett. **79** (1997) 3544] [hep-ph/9610260].

[52] W. Celmaster and R. J. Gonsalves, Phys. Rev. D **20** (1979) 1420, Phys. Rev. Lett. **42** (1979) 1435, P. Pascual and R. Tarrach, Nucl. Phys. B **174** (1980) 123 [Erratum-ibid. B **181** (1981) 546].

[53] B. R. Webber, JHEP **9810** (1998) 012. [hep-ph/9805484].

[54] G. Rodrigo and M. Ciafaloni, Nucl. Phys. Proc. Suppl. **99A**, 200 (2001) [hep-ph/0010216].

[55] G. Rodrigo and A. Santamaria, Phys. Lett. B **313**, 441 (1993) [hep-ph/9305305].

[56] G. Rodrigo, A. Pich and A. Santamaria, Phys. Lett. B **424**, 367 (1998) [hep-ph/9707474].

[57] A. A. Alves, Jr. *et al.* [LHCb Collaboration], JINST **3** (2008) S08005.

[58] A. D. Martin, W. J. Stirling, R. S. Thorne and G. Watt, Eur. Phys. J. C **63** (2009) 189-285 [hep-ph/0901.0002].

[59] G. Chachamis, A. Sabio Vera, C++ BFKL Monte Carlo code.

[60] G. Chachamis, M. Deak, A. Sabio Vera and P. Stephens, Nucl. Phys. B **849**, 28 (2011) [arXiv:1102.1890 [hep-ph]].

[61] G. Chachamis and A. Sabio Vera, Phys. Lett. B **709**, 301 (2012) [arXiv:1112.4162 [hep-th]].

[62] G. Chachamis and A. Sabio Vera, Phys. Lett. B **717**, 458 (2012) [arXiv:1206.3140 [hep-th]].

[63] G. Chachamis, A. Sabio Vera and C. Salas, Phys. Rev. D **87**, no. 1, 016007 (2013) [arXiv:1211.6332 [hep-ph]].